Osteology of a New Specimen of Macrocnemus aff. M. fuyuanensis (Archosauromorpha, Protorosauria) from the Middle Triassic of Europe: Potential Implications for Species Recognition and Paleogeography of Tanystropheid Protorosaurs

Jaquier, Vivien P ; Fraser, Nicholas C ; Furrer, Heinz ; Scheyer, Torsten M

DOI: https://doi.org/10.3389/feart.2017.00091

Cranial shape variation in jacarean caimanines (Crocodylia, Alligatoroidea) and its implications in the taxonomic status of extinct species: the case of *Melanosuchus fisheri*

Christian Foth[1,2], María Victoria Fernandez Blanco[3], Paula Bona[3], Torsten M. Scheyer[4]

1-Department of Geosciences, University of Fribourg/Freiburg, Chemin du Musée 6 CH-1700 Fribourg, Switzerland.

2-Staatliches Museum für Naturkunde, Rosenstein 1, D-70191 Stuttgart, Germany.

3-División Paleontología Vertebrados, Museo de La Plata-Universidad Nacional de La Plata. Paseo del Bosque s/n. 1900, La Plata, Buenos Aires, Argentina. Consejo Nacional de Investigaciones Científicas y Técnicas (CONICET).

4-Paläontologisches Institut und Museum, Universität Zürich, Karl Schmid-Strasse 4, CH-8006 Zürich, Switzerland.

Corresponding author:

Christian Foth

Staatliches Museum für Naturkunde, Rosenstein 1, D-70191 Stuttgart, Germany

christian.foth@gmx.net

Abstract

Melanosuchus niger (Crocodylia, Alligatoroidea) is one of the six living caimanine species widely distributed throughout the Amazon River basin today. Although there is only one extant species of *Melanosuchus*, fossil material assigned to this genus, represented by *M. fisheri*, has been reported from the late Miocene in South America. However, the validity of this taxon has been questioned and a recent investigation indicates that the referred specimen of *M. fisheri* (MCZ 4336) actually belongs to *Globidentosuchus brachyrostris*, while those diagnostic characters present in the holotype (MCNC 243) fall into the spectrum of intraspecific variation of *M. niger*. Here, we compare the skull shape of the holotype of *M. fisheri* with the ontogenetic series of the four jacarean species (*M. niger, Caiman yacare, Caiman crocodilus* and *Caiman latirostris*) using 2D geometric morphometric analyses in two different views. The analyses indicate that MCNC 243 falls into the morphospace of *M. niger* and *C. latirostris*. Despite strong shape similarities between juveniles of *C. latirostris* and MCNC 243, further anatomical comparisons reveal notable differences between them. In contrast, no concrete anatomical differences can be found between MCNC 243 and *M. niger*, although shape analyses indicate that MCNC 243 is relatively robust for its size. Thus, this study is able to confirm that the genus *Melanosuchus* was present in the late Miocene, but it still remains unclear if MCNC 243 should be treated as a junior synonym or probably a sister species of *M. niger*. Its Miocene age favors the second option, but as the shape analyses were also not able to extract any diagnostic characters, it should be retained as *Melanosuchus* cf. *niger*.

Keywords: Amazonia, Caimaninae, geometric morphometrics, Neogene, South America

Graphical Abstract

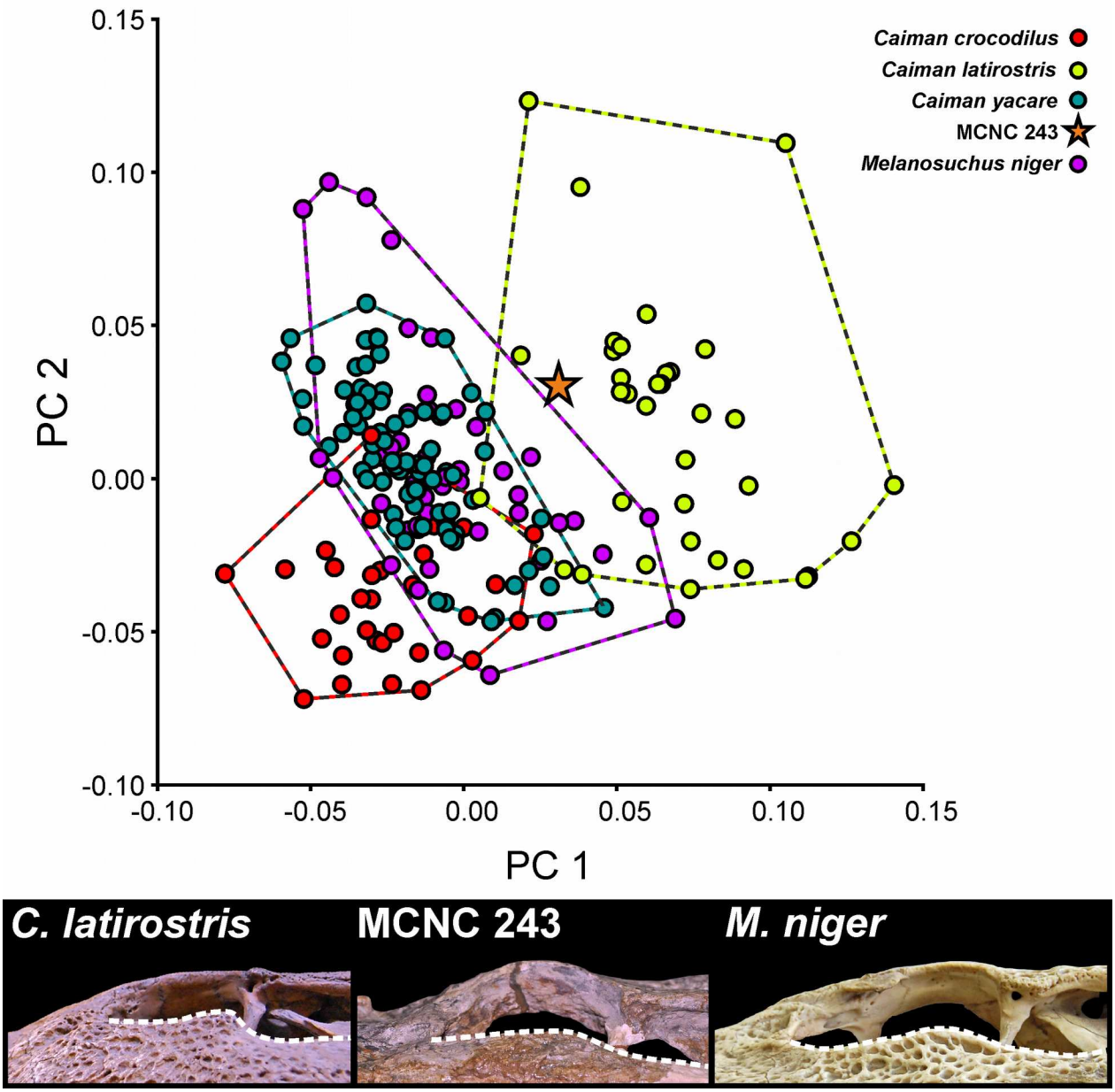

A comparison of the skull shape of the fossil caiman MCNC 243 with four jacarean caimans indicates that MCNC 243 falls into the morphospace of *Melanosuchus niger* and *Caiman latirostris*, while orbit shape and size supports an affiliation with the genus *Melanosuchus*.

1. Introduction

The black caiman (*Melanosuchus niger* Spix, 1825) is the largest extant member of Alligatoroidea, with adult males that can exceed 4–5 m in length and females with a mean adult total length of 2.8 m (Brazaitis, 1973; Thorbjarnarson, 2010). Within Alligatoroidea, phylogenetic analyses place *M. niger* closer to the genus *Caiman* Spix, 1825 than to *Paleosuchus* Gray, 1862, forming the clade Jacarea (e.g., Brochu, 1999, 2003, 2010; Oaks, 2011; Scheyer *et al.*, 2013; Salas-Gismondi *et al.*, 2015). Today, *M. niger* is widely distributed throughout the Amazon River basin, but fossil discoveries allow researchers to trace the history of the genus back to the Late Miocene (Medina, 1976; Sánchez-Villagra and Aguilera, 2006; Scheyer and Delfino, 2016). Two fossil skulls (the holotype MCNC 243 and referred specimen MCZ 4336) from the Urumaco Formation of Venezuela were described as *Melanosuchus fisheri* Medina, 1976 (Figure 1), but their validity was called into question as both skulls are fairly damaged and taphonomically deformed, making a proper diagnosis impossible (Brochu, 1999). A recent reinvestigation of the skull material described by Medina (1976) came to the conclusion that the holotype and the referred specimen are different species, and MCZ 4336 shares a number of similarities with the basal caimanine *Globidentosuchus brevirostris* Scheyer *et al.*, 2013 from the same formation (Bona *et al.*, in press). As some of the diagnostic characters of *M. fisheri* are based on this referred specimen, this result has a significant impact on the validity of the latter species. In contrast, the holotype specimen could be clearly classified as a jacarean caimanine, but due to its bad preservation neither a certain assignment to the genus *Melanosuchus* nor a valid diagnosis of *M. fisheri* could be given on the basis of the anatomical comparison (Bona *et al.*, in press).

Thus, the aim of this study is to test the taxonomic status of *M. fisheri* based on the holotype (MCNC 243) by comparing its cranial shape with the cranial ontogenetic series of the four

jacarean caimanine species; *Caiman yacare* Daudin, 1802, *Caiman crocodilus* Linnaeus, 1758, *Caiman latirostris* Daudin, 1802 and *M. niger,* performing 2D geometric morphometric analyses (GMA). Together with further anatomical comparison we want to investigate if MCNC 243 can be assigned to the genus *Melanosuchus* and if the species *M. fisheri* can be diagnosed with help of shape differences.

1.1. *Institutional abbreviations*

AMU-CURS, Colección de Paleontología de Vertebrados de la Alcaldía de Urumaco, Estado Falcón, Venezuela; **FML**, Fundación Miguel Lillo, Tucumán, Argentina; **MACN**, Museo Argentino de Ciencias Naturales “Bernardino Rivadavia”, Buenos Aires, Argentina; **MCNC**, Museo de Ciencias Naturales de Caracas, Venezuela; **MCZ**, Museum of Comparative Zoology, Harvard University, USA; **MFA**, Museo Provincial de Ciencias Naturales "Florentino Ameghino", Santa Fé, Argentina; **MLP,** Museo de La Plata, Buenos Aires, Argentina; **ZSM,** Zoologische Staatssammlung München, Germany.

2. Materials and methods

2.1. *Geometric morphometric analyses of jacarean caimanine skulls*

Geometric morphometrics is a powerful tool for taxonomic identification (e.g. Zelditch *et al*., 2012) and has been previously applied to study cranial shape variation in crocodylians and their ancestors. For instance, Piras *et al.* (2010) and Watanabe and Slice (2014) studied the ontogenetic variation in the crocodylian skull, while Monteiro *et al*. (1997), Fernandez Blanco *et al*. (2014),

Foth *et al.* (2015) and Okamoto *et al*. (2015) focussed similar studies particularly on caimanines. In addition, Hastings and Hellmund (2016) studied the cranial shape diversity of fossil crocodylians from the Geiseltal Lagerstätte in Germany, while Young *et al.* (2010), Stubbs *et al*. (2013), Foth, Ezcurra *et al.* (2016) and Wilberg (2017) performed geometric morphometric and disparity analyses on the cranial shape of crocodylian ancestors during the Mesozoic.

For the geometric morphometric analyses, we examined the skull of the holotype of *Melanosuchus fisheri* (MCNC 243) and the four living species of jacarean Caimaninae: *Melanosuchus niger, Caiman yacare*, *Caiman crocodilus* and *Caiman latirostris* (following the taxonomy of Brochu, 1999). All skulls were photographed in dorsal and left lateral view as described by Pearcy and Wijtten (2010), resulting in 194 specimens in dorsal view (78 of *C. yacare*, 35 of *C. latirostris*, 33 of *C. crocodilus*, 47 of *M. niger* and MCNC 243) and 193 specimens in lateral view (76 of *C. yacare*, 35 of *C. latirostris*, 34 of *C. crocodilus*, 47 of *M. niger* and MCNC 243) (Supp. Table 1), including individuals of different postnatal ontogenetic stages for each species. Depending on the availability in scientific collections the ratio of premature individuals varies roughly between 10.6% (*M. niger*) and 68.4% (*C. yacare*). As no specific age data is available, in general we used half of the maximum centroid size in each species as a rough threshold for defining the stage of maturity. This threshold is based on the observation in *Alligator mississippiensis*, in which sexual maturity is reached at about half of the average maximum body length (see Wilkinson and Rhodes, 1997).

The digital images of caiman skulls were compiled into a *tps* file using the program *tpsUtil 1.44* (Rohlf, 2004). Skull shape was captured in dorsal view using 28 landmarks and 2 semi-landmarks (Supp. Table 2), and in lateral view using 16 landmarks and 6 semi-landmarks (Supp. Table 3; Supp. Figure 1). The different landmarks include homologies of Type I (intersection of

sutures), Type II (maximum and minimum of curvatures) and Type III (extreme or constructed points) following the definition of Bookstein (1991). Landmarks and semi-landmarks were digitized using the software *tpsDig 2.14* (Rohlf, 2005). For dorsal view, we chose an unilateral configuration (left side) because mirroring landmarks would not add more shape information (Young *et al.*, 2010), but in contrast inflate the degrees of freedom in the statistical analyses (Pierce *et al.*, 2008).

In order to include damaged specimens and increase sample size, we estimated missing landmarks for a handful of specimens using the function *estimate.missing* in the package '*geomorph*' (Adams and Otárola-Castillo, 2013) with *R 3.1.2* (R Development Core Team, 2011). This function interpolates the thin-plate spline of a reference specimen, which is based on all specimens with complete landmarks, in order to map the locations of missing landmarks on the target specimens (Gunz *et al.*, 2009). The number of missing landmarks varies from one (for both views) to six (for lateral view) and one to 15 (for dorsal view). The amount of affected specimens varies between 10.6% (for *M. niger* in dorsal view) to 40.5% (for *C. latirostris*) (see Supp. Table 1). This procedure was done for each species separately to avoid misplacements of landmarks due to interspecific variation. The position of reconstructed landmarks was controlled for each specimen afterwards.

In the next step, the datasets of each species were combined into one large file and loaded in *R*. Using the package '*geomorph*' the landmark coordinates were superimposed with help of Generalized Procrustes Analysis (GPA), which minimizes shape variation related to scale, translation (i.e., position) and rotation, leaving only shape variation (Rohlf and Slice, 1990). Because semi-landmarks possess lesser degrees of freedom than ordinary landmarks, it can be appropriate to minimize their impact on shape analyses. To do so, semi-landmarks were slid

along the line-tangent to the curve during superimposition, minimizing the bending energy of deformation in the thin-plate spline (Zelditch *et al.*, 2012).

Before applying the Procrustes superimposed data to PCA and other statistical analyses, we regressed Procrustes distance against Euclidean distance for each landmark pair, using the program *tpsSmall 1.2* (Rohlf, 2003). This procedure estimates the amount of distortion when the Procrustes data, which lie within a curved space (i.e., Kendall's shape space), is projected onto the Euclidean space (Dryden and Mardia, 1998). For both datasets, correlation was found to be 1, indicating that distortion is minimal, and that all results of subsequent analyses are confident in respect of geometrical projection. Data were exported to *MorphoJ 1.06d* (Klingenberg, 2011) where a principal component analysis (PCA) was performed by generating a covariance matrix. To explore shape changes along ontogeny, we performed a multivariate regression on the Procrustes coordinates against log-transformed centroid size. A verification of correlations indicates the presence of an allometric signal in the data, and produces a set of residual coordinates for which allometric variation is reduced. In addition, a pooled species within-group multivariate regression, which uses the deviation of observations of the average of variables of each species instead of the deviation from the grand mean of all species (Klingenberg, 2009), was conducted. Afterwards, we analyzed the slopes of ontogenetic series performing a one-way ANCOVA on the basis of an *F* test in *PAST v. 3.05* (Hammer *et al.*, 2001). This performance allows testing if ontogenetic trajectories show different allometric growth, which is characterized by differences in slope and intercept. Finally, we reran a PCA on the basis of (pooled and un-pooled) non-allometric residuals from the regression tests, and compared the distribution of species to the original PCA (see above).

All datasets were tested for normality, using the Henze-Zirkler's, Mardia's and Royston's multivariate normality (MVN) test in *R* (Supp. Table 4), which are integrated in the *R*-package '*MVN*' (Korkmaz *et al.*, 2014). The Henze-Zirkler's MVN test is based on a non-negative functional distance, which measures the distance between two distribution functions. The Mardia's MVN test is based on a multivariate projection of skewness and kurtosis, while the Royston's MVN test uses Shapiro-Wilk/Shapiro-Francia statistics. If *p*-values of each test are 0.05 or higher, the data is normally distributed. Results were further visualized by a Chi-Square Q-Q plot (Supp. Figure 2).

In order to test whether different extant caimanine species overlap with each other or are significantly separated from each other in morphospace, we performed a multivariate analysis of variance (MANOVA) and a nonparametric multivariate analysis of variance (npMANOVA, also called perMANOVA) in *PAST*, and a Discriminant Function Analysis (DFA) and a Canonical Variate Analysis (CVA) in *MorphoJ*. MANOVA is a parametric test requiring normal distribution of data that searches equality of multivariate means within different groups, indicating a potential overlapping in morphospace (Hammer and Harper, 2006). In contrast, npMANOVA tests the significance of the distribution of groups on the basis of permutation (10,000 replications) and Euclidean distance (as one of several possible distance measures), and does not require normal distribution (Anderson, 2001; Hammer and Harper, 2006). In both cases, the spatial relationship of species relative to each other is expressed by a *p*-value, which was Bonferroni corrected by multiplying the *p*-values with the number of comparisons. In contrast, DFA and CVA try to project a multivariate dataset down to one dimension by maximizing the separation between two (DFA) or more groups (CVA) (Hammer and Harper, 2006) on the basis of Procrustes (= Euclidean) distances and Mahalanobis distances. Whereas the former is a measure of the absolute

between group mean distances, the latter incorporates additional within-group variation to the calculation (Drake, 2011). Significance level was given by a *p*-value, which is based on a permutation (10,000 replications). The overlap and separation of species within morphospace was tested on the basis of Procrustes coordinates and non-allometric residuals of both the pooled and un-pooled multivariate regressions. If the *p*-values of each test are 0.05 or smaller, a significant separation between two groups within morphospace can be assumed.

2.2. Position of **Melanosuchus fisheri** *with jacarean caimanines*

After investigating the general shape variation within jacarean caimanines, we explored the position of *Melanosuchus fisheri* relative to other Caimaninae in morphospace by calculating the relative probability (deterministic model; see Benson *et al.*, 2011) on the basis of principal components sourcing on both Procrustes coordinates and non-allometric residuals (pooled and un-pooled). For that, principal components were conducted with the broken stick method (Jackson, 1993), which determines those principal components (PCs) with significant shape variation. In the next step, we estimated the centroids of the morphospace of each extant species on the basis of the median and average of the PCs, defining the mean shapes of each species. Afterwards, we estimated the Euclidian distance of MCNC 243 to each species centroid. The similarity of MCNC 243 to other caimanine species is expressed by the relative probability, which is the normalized inverse distance of MCNC 243 and each species centroid (see Benson *et al.*, 2011; Foth, Rabi *et al.*, 2017). The results were compared with the outcome of the DFA and CVA (see above).

3. Results

3.1. *Skull shape variation of jacarean caimanines*

For the dorsal view, significant shape variation is defined by the first four PCs, which explain 73.0 % of total shape variation (PC1=38.5%, PC2=17.5%, PC3=9.4%, PC4=7.6%). Negative values of PC1 (Figure 2B) describe specimens with a short snout (LM 1 and LM 29), short and wide naris (LM 2 to LM 4) and nasal (LM 5 to LM 8), large, anteriorly displaced orbit (LM 10 to LM 13 and LM 25), elongated supratemporal fenestra (LM 14 to LM 17), large, laterally displaced infratemporal fenestra (LM 23 to LM 25 and LM 13), posteriorly displaced posterior margin of the skull table (LM 18 to LM 21) and a posteromedial displacement of the posterior point of the quadrate-quadratojugal suture (LM 22). The anterior end of the nasal reaches into the naris (LM 5 and 4, respectively). The cranial outline is wide. Positive values (Figure 2C) show specimens with a long snout (LM 1 and LM 29), long and narrow naris (LM 2 to LM 4) and nasal (LM 5 to LM 8), small, posteriorly displaced orbit (LM 10 to LM 13 and LM 25), shortened supratemporal fenestra (LM 14 to LM 17), small, anteromedially displaced infratemporal fenestra (LM 23 to LM 25 and LM 13), anteriorly displaced posterior border of the skull table (LM 18 to LM 21) and an anterolateral displacement of the posterior point of the quadrate-quadratojugal suture (LM 22). The anterior end of the nasal does not contact the naris (LM 5 and LM 4, respectively). The cranial outline is narrow.

Regarding PC2, negative values of this component (Figure 2D) account for specimens with a short snout (LM 1 and LM 29), short and wide naris (LM 2 to LM 4), large and wide nasal (LM 5 to LM 8), short and wide orbit (LM 10 to LM 13 and LM 25), small, medially displaced supratemporal fenestra (LM 14 to LM 17), wide infratemporal fenestra (LM 23 to LM 25 and

LM 13), concavely shaped posterior margin of the skull table (LM 18 to LM 21) and a posterolateral displacement of the posterior point of the quadrate-quadratojugal suture (LM 22). The posterior contact between both nasals and the most anterior point of the frontal (LM 8 and LM 9, respectively) are separated. The anterior end of the nasal reaches into the naris (LM 5 and LM 4, respectively). The cranial outline is wide. Positive values of this component (Figure 2E) display a long snout (LM 1 and LM 29), long and narrow naris (LM 2 to LM 4), narrow and slightly short nasal (LM 5 to LM 8), large, laterally displaced orbit (LM 10 to LM 13 and LM 25), large, laterally displaced supratemporal fenestra (LM 14 to LM 17), narrow and slightly large infratemporal fenestra (LM 23 to LM 25 and LM 13), almost straight (posteriorly displaced) posterior margin of the skull table (LM 18 to LM 21) and an anteromedial displacement of the posterior point of the quadrate-quadratojugal suture (LM 22). The posterior contact between both nasals and the most anterior point of the frontal (LM 8 and LM 9, respectively) are very close. The anterior end of the nasal does not contact the naris (LM 5 and LM 4, respectively). The cranial outline is basically narrow.

For lateral view, the first three principal components contain significant shape variation and explain 72.4 % of total shape variation (PC1=33.1%, PC2=25.1%, PC3=14.2%). Shape changes associated with negative values of PC1 (Figure 3B) show dorsoventrally compressed skulls with a long snout (LM 1), large orbit (LM 12 to LM 17), tall and posteroventrally displaced infratemporal fenestra (LM 11 to LM 13), anterodorsal displaced posterior contact between the quadrate and quadratojugal (LM 8) and an anteroventral displacement of the most posterodorsal point of the squamosal (LM 10). Positive values (Figure 3C) represent high skulls with a short snout (LM 1), small orbit (LM 12 to LM 17), low and anterodorsally displaced infratemporal fenestra (LM 11 to LM 13), posteroventrally displaced posterior contact between the quadrate

and quadratojugal (LM 8), and a posterodorsal displacement of the most posterodorsal point of the squamosal (LM 10).

Regarding PC2, negative values of this component (Figure 3D) account for skulls with a long and deep snout (LM 1 to LM 4, LM 18, LM 19 and LM 22) relative to the low postrostral region (LM 5 to LM 17, LM 20 and LM 21), which is compressed, a small orbit (LM 12 to LM 17) and infratemporal fenestra (LM 11 to LM 13), anterodorsally displacement of the posterior contact between the quadrate and quadratojugal (LM 8) and an anteroventral displacement of the most posterodorsal point of the squamosal (LM 10). The lowest point of the maxilla (LM 4) is anteroventrally displaced and the contact of maxilla and premaxilla (LM 3) is anterodorsally displaced. Positive values of this component (Figure 3E) include skulls with a short and tapering snout (LM 1 to LM 4, LM 18, LM 19 and LM 22) relative to the high postrostral region (LM 5 to LM 17, LM 20 and LM 21), an enlarged orbit (LM 12 to LM 17) and infratemporal fenestra (LM 11 to LM 13), posteroventrally displaced posterior contact between the quadrate and quadratojugal (LM 8), and a posterodorsal displacement of the most posterodorsal point of the squamosal (LM 10). The lowest point of the maxilla (LM 4) is posterodorsally displaced and the contact of the maxilla and premaxilla (LM 3) is posteroventrally displaced.

3.2. *Morphospace occupation of jacarean caimanines*

For dorsal view, specimens are mainly distributed into two groups separated along the first and second PC axes (Figure 2A). *Caiman latirostris* is well separated from the other species in the area determined by negative values of both PC1 and PC2. *Melanosuchus niger*, *Caiman yacare* and *Caiman crocodilus* overlap with each other in the remaining morphospace. Here, *M. niger* is

separated from *C. crocodilus* with respect to PC1, while *C. yacare* overlaps with both species. If allometric shape variation is excluded from the data, the morphospace is similar to the former case but the overlapping of *M. niger* with *C. yacare* and *C. crocodilus* is less intensive (Supp. Figure 2 A). Pooling species for species affiliation results in a stronger separation of *M. niger* and *Caiman latirostris* from other species, while *C. yacare* and *C. crocodilus* remain overlapping. (Supp. Figure 2 B).

In lateral view, PCA also reveals that species are mainly clustered into two groups separated along the first and second PC axes (Figure 3A). *C. latirostris* is well separated from other Caimaninae toward the most positive values of PC1 but overlaps marginally with *M. niger* and *C. yacare*. In the second cluster, toward the negative values of PC1, *M. niger* and *C. yacare* overlap with each other with respect to both PC axes. *C. crocodilus* is more separated from other species, overlapping partly with *M. niger* and *C. yacare*. Non-allometric data reveals a similar distribution of species within morphospace, although *M. niger* and *C. yacare* are better separated from each other with respect to the second PC axis. When data are additionally pooled, the separation between *M. niger* and *C. yacare* is enhanced (Supp. Figure 2C), whereas *C. yacare* overlaps more strongly with *C. crocodilus*.

For both views, all statistical tests reveal that *M. niger*, *C. yacare*, *C. crocodilus* and *C. latirostris* occupy distinct areas in morphospace and can be distinguished significantly from each other by shape (Supp. Table 5, 10).

3.3. *Ontogenetic variation of jacarean caimanines*

In dorsal view, based on the regression analysis between Procrustes coordinates and log-transformed centroid size, allometric size variation explains 10.67% of total shape variation (*p*-value < 0.0001) for raw data (Figure 4), and 28.08% when the data is pooled for species. Main ontogenetic changes are included in the shape variation described by PC1 and PC3. In general, juvenile caimanines (Figure 4B) share a short snout (LM 1 and LM 29), naris (LM 2 to LM 4) and nasal (LM 5 to LM 8), wide and short orbit (LM 10 to LM 13 and LM 25), elongated supratemporal fenestra (LM 14 to LM 17), laterally displaced infratemporal fenestra (LM 23 to LM 25 and LM 13), posteriorly displaced posterior border of the skull table (less concave) (LM 18 to LM 21) and an anteromedially displaced posterior point of the quadrate-quadratojugal suture (LM 22). The anterior end of the nasal contacts the naris (at the same level of the premaxilla) (LM 5 and LM 4, respectively) (Figure 4B). Adult specimens (Figure 4C) show a long snout (LM 1 and LM 29), naris (LM 2 to LM 4) and nasal (LM 5 to LM 8), long and narrow orbit (LM 10 to LM 13 and LM 25), shortened supratemporal fenestra (LM 14 to LM 17), medially displaced infratemporal fenestra (LM 23 to LM 25 and LM 13), anteriorly displaced (more concave) posterior border of the skull table (LM 18 to LM 21) and a posterolateral displacement of the posterior point of the quadrate-quadratojugal suture (LM 22). The anterior end of the nasal almost reaches the posterior border of the naris (LM 5 and 4, respectively) (Figure 4C). All species show very similar ontogenetic trajectories (Figure 4), although *Caiman latirostris* differs from *Melanosuchus niger* (for un-pooled regression) and *Caiman crocodilus* (for pooled regression) (Table 1).

In lateral view, allometric size variation explains 17.69% of total shape variation (*p*-value < 0.0001) for raw data (Figure 5), and 33.01% when data is pooled. Main ontogenetic changes are

included in the shape variation described by PC2 and PC3. Juvenile specimens (Figure 5B) share a short and low snout (LM 1 to LM 4, LM 18, LM 19 and LM 22), large orbit (LM 12 to LM 17) and infratemporal fenestra (LM 11 to LM 13), anteroventrally displaced posterior contact between the quadrate and quadratojugal (LM 8) and a posteroventral displacement of the most posterodorsal point of the squamosal (LM 10). The orbital region (LM 14, LM 15 and LM 20) is dorsally expanded in relation to the snout, the lowest point of the maxilla (LM 4) is posterodorsally displaced and the contact of the maxilla and premaxilla (LM 3) is posteriorly displaced (Figure 5B). Adult specimens (Figure 5C) show a slightly long and tall snout (LM 1 to LM 4, LM 18, LM 19 and LM 22), small orbit (LM 12 to LM 17) and infratemporal fenestra (LM 11 to LM 13), posterior contact between the quadrate and quadratojugal (LM 8) that is dorsally displaced and an anterior displacement of the most posterodorsal point of the squamosal (LM 10). The orbital region (LM 14, LM 15 and LM 20) is flattened dorsally, the lowest point of the maxilla (LM 4) is anteroventrally displaced and the contact of the maxilla and premaxilla (LM 3) is anteriorly displaced (Figure 5C). The un-pooled allometric trajectories of *M. niger* resemble that of *C. latirostris* and *Caiman yacare*, while *C. crocodilus* has a significantly lower slope than *M. niger*, *C. latirostris* and *C. yacare*. *C. yacare* differs significantly from *C. latirostris*. When data is pooled, most trajectories become similar, although *M. niger* differs significantly from *C. crocodilus* as the former has a higher slope than the latter (Table 1).

3.4. *The affiliation of Melanosuchus fisheri*

Based on its size in dorsal view, MCNC 243 appears within the biggest size classes of *C. latirostris*, *C. yacare* and *C. crocodilus*, but within the intermediate sizes of *M. niger* (Figure 3A).

In this view, *Melanosuchus fisheri* lies in the overlap area of the morphospaces of *Melanosuchus niger* and *Caiman latirostris*, but also close to *Caiman yacare and Caiman crocodilus* (Figure 2A). For non-allometric data, the shape of the morphospace of each species is retained, but MCNC 243 lies deeper within the morphospace of *M. niger* (Supp. Figure 2). For pooled, non-allometric data, MCNC 243 lies isolated in the middle of the morphospace, but is closer to *M. niger* than all others (Supp. Figure 2). Based on the relative probability, MCNC 243 is closer to *M. niger* in all cases, except for the average-based species centroids of non-allometric residuals, where MCNC 243 is closer to *C. latirostris*. In direct comparison to *M. niger* and *C. latirostris*, MCNC 243 resembles *M. niger*, except when non-allometric residuals are used (Table 2). DFA and CVA frequently fail to separate MCNC 243 from *M. niger* and *C. latirostris*, although most cases favor an association of MCNC 243 with the black caiman (Table 3).

In lateral view, MCNC 243 clusters in the overlap area of the morphospaces of *M. niger* and *C. latirostris* for Procrustes-based (Figure 3A) and non-allometric data (Supp. Figure 2), while for pooled, non-allometric data, it lies isolated between *C. latirostris*, *M. niger* and *C. yacare* (Supp. Figure 2). Based on relative probability, MCNC 243 resembles *M. niger*, when non-allometric data is used, whereas pooling species results in a closer relationship with *C. latirostris*. For Procrustes-based principal components MCNC 243 is closer to *M. niger* for average-based species centroids, whereas the median-based centroids lead to a closer relationship with *C. latirostris*. In direct comparison to *M. niger* and *C. latirostris*, MCNC 243 resembles *M. niger*, except when species are pooled (Table 4). As in dorsal view, DFA and CVA fail to separate MCNC 243 from *M. niger* and *C. latirostris*, but in contrast to the former case, MCNC 243 is found more often together with the broad-snouted caiman.

4. Discussion

Shape analyses reveal that all extant jacarean caimanine species can be separated from each other on a significant level based on cranial shape. Although shape data is not normally distributed (Supp. Table 4, Supp. Figure 3), CVA, DFA, MANOVA and npMANOVA produce similar results for the separation of different species (Supp. Table 5-10). As npMANOVA does not require normality, we treat the similar outcomes of the other tests as robust. Although different in shape, the ontogenetic trajectories of *Caiman* and *Melanosuchus* species are, however, generally similar, especially in dorsal view, meaning that the skulls of each species studied undergo similar allometric shape changes during growth (see also Watanabe and Slice, 2014; Fernandez Blanco *et al.*, 2014; Foth *et al.*, 2015). In consequence, differences in cranial shape are simply given by size, which depends on the length (i.e., the duration of growth, found in dorsal and lateral view) and the starting point of the trajectories (i.e., the size of the hatchling, found only in dorsal view). Only *Caiman crocodilus* is slightly different from the other species, showing fewer allometric shape changes.

Within morphospace, the holotype of *Melanosuchus fisheri* (MCNC 243) is closer to *Melanosuchus niger* and *Caiman latirostris* than to *Caiman yacare* and *C. crocodilus*, which is verified by multiple different statistical analyses. Here, it is evident that MCNC 243 is closer to *M. niger* for dorsal view, while it shows some more similarities to *C. latirostris* in lateral view. This result is in agreement with previous morphology-based phylogenetic analyses, where *M. niger* and *C. latirostris* form a clade, excluding *C. yacare* and *C. crocodilus* (Poe, 1996; Brochu, 1999, 2004, 2011; Hastings *et al.*, 2016). MCNC 243 shares with *M. niger* and *C. latirostris* some discrete characters (or rather falls within the intraspecific morphological range of variation of the two extant taxa) that include: presence of 13 maxillary teeth and a strong transversal preorbital

ridge (Scheyer and Delfino, 2016; also present in *C. crocodilus*). In *C. latirostris*, the ridge is usually continuous and broadly U-shaped (as in MCNC 243), while most individuals of *M. niger* show an interruption by the frontals, giving it a W-shaped (double U-shaped) appearance. However, individual variation also includes W-shaped ridges in *C. latirostris* and U-shaped ridges in *M. niger*. In MCNC 243, the prefrontals contact each other, while in the majority of individuals of *M. niger* and *C. latirostris* these bones are separated from each other by the frontals. However, due to individual variation, the former condition can be occasionally found in both extant species. Furthermore, the skull roof table of MCNC 243 possesses a straight posterior margin. This character is usually highly variable in both extant species, varying from straight to concave in *M. niger* and straight to convex in *C. latirostris*. Thus, the straight condition found in MCNC 243 can be found in both extant taxa, too.

Despite the similarities in morphology and close morphospace occupation with *C. latirostris*, MCNC 243 can be affiliated with the genus *Melanosuchus* as originally proposed by Medina (1976) for several reasons. Within morphospace, most specimens of *C. latirostris* plotting close to MCNC 243 (dorsal view: MACN 30565*, MACN 30611*, MLP R 5812*, FML 23627; lateral view: MLP R5802, MLP R 5803, MLP R5804*, MLP R5808, MLP R5809, MLP R5811*, MACN 30567, ZSM 3003/0*, MFA-ZV-Croc.O.8; *specimens with reconstructed landmarks) are primarily juvenile individuals, which are significantly smaller (ranging from 16 to 68% of the centroid size of MCNC 243). Thus, shape similarities between MCNC 243 and *C. latirostris* are based primarily on juvenile characters, including the relatively large orbit and a moderately broad rostrum. During ontogeny, however, the orbits of *C. latirostris* become relatively smaller, while the snout gets broader, representing an extreme within extant crocodylians (Mook, 1921; Kälin, 1933; Bona and Desojo, 2011; Figure 1A). Besides, MCNC 243 differs from *C. latirostris* in

having oval-shaped orbits (Figure 1B) and a gently curved orbital margin of the jugal (Figure 1E). In *C. latirostris* the orbits are rather round (Figure 1A) and the posterior half of the jugal orbital margin possesses a distinct kink (Figure 1D). In contrast, the closest individuals of *M. niger* are about the same size or larger than MCNC 243 (ranging from 87 to 245% of the centroid size of MCNC 243). Like *M. niger* specimens of the same size range, MCNC 243 has enlarged, oval-shaped orbits (Figure 1B) and similar proportions of the rostrum. Enlarged orbits are a characteristic of *M. niger* and represent another extreme within recent crocodylians (Mook, 1921; Kälin, 1933; Figure 1C). Furthermore, the orbital margin of the jugal is similar in MCNC 243 and *M. niger* in that they both lack the distinct kink of *C. latirostris* (Figure 1E, F).

If MCNC 243 can be assigned to the genus *Melanosuchus* the next question is whether it belongs to *M. niger* or represents its own species, namely *M. fisheri*. Unfortunately, due to the poor preservation of this specimen there are no characters that allow a proper diagnosis. As found by Bona *et al*. (in press), most characters of the original diagnosis listed by Medina (1976) cannot be evaluated for the holotype due to its state of preservation (e.g., size of the suborbital and external mandibular fenestrae; robustness of the mandible) and preparation (e.g., shape of the interorbital bar), while other diagnostic characters fall within the range of intraspecific variation of *M. niger* (e.g., robustness of the skull and the snout; intensity of the preorbital ridges on snout; shape of the central portion of posterior border of skull roof table). In addition, those diagnostic features that actually separate *M. fisheri* from *M. niger* (e.g., number of maxillary teeth; size of the suborbital and external mandibular fenestrae; robustness of the mandible) are based on the referred specimen (MCZ 4336; Medina, 1976), which actually belongs to *Globidentosuchus brachyrostris* (Bona *et al*., in press). In the absence of any discrete morphological features that allow a final taxonomic conclusion, it is more correct to consider MCNC 243 as *M. niger*, *Melanosuchus* cf.

niger or even *Melanosuchus* sp. (see Bona *et al.*, in press). The morphometric analyses reveal that MCNC 243 is nested at the margin of the *Melanosuchus niger* morphospace, and has a relatively robust morphology for its size (see also AMU-CURS-234; Scheyer and Delfino, 2016), which is the only character of the original diagnosis from Medina (1976) that is actually present in this specimen. However, treating the robustness as an extreme shape for *M. niger*, MCNC 243 could still be assigned to the extant species. However, together with the late Miocene age (c. 6–8 mya) of MCNC 243, the relative robustness of the skull makes an assignment to the extant species *Melanosuchus niger* still problematic, so that we classify MCNC 243 as *Melanosuchus* cf. *niger*.

The marginal position of MCNC 243 relative to the morphospace of *M. niger* (especially in lateral view) indicates a possible variation of the morphospace size and/or position of this lineage through time and maybe a stronger overlapping with the morphospace of *C. latirostris* in the past (assuming similar morphospace variations). The closeness of MCNC 243 to the *C. latirostris* morphospace indicates a closer relationship between *Melanosuchus* and *C. latirostris* (see above), where *Melanosuchus* is nested within the genus *Caiman* (Poe, 1996; Brochu, 1999, 2004, 2011; Hastings *et al*., 2016). If this relationship can be verified by future molecular-based phylogenetic analyses, the genus *Melanosuchus* will need to be synonymized with *Caiman*. However, for the moment all molecular studies favour a relationship, in which *M. niger* is the sister species to all extant *Caiman* species, with *C. latirostris* being closest to the root of the genus (Poe, 1996; Hrbek et al., 2008; Oaks, 2011), causing no conflict in present caimanine taxonomy.

5. Conclusions

The present study reveals that the holotype of *Melanosuchus fisheri* shares more similarities with the extant *Melanosuchus niger* than the other three jacarean caimanines. These similarities could be found on two levels: overall shape (this study) and discrete morphological features (this study; Bona *et al*., in press). As MCNC 243 is relatively robust for its size and represents an extreme shape for *Melanosuchus*, it is uncertain if it should be assigned to *M. niger* or as a potential sister species. Its Miocene age, however, favors the second option, but as no diagnostic characters can be established it should be retained as *Melanosuchus* cf. *niger*. The robust affinity of MCNC 243 indicates a close relationship between *Melanosuchus* and *Caiman latirostris*, as predicted by morphology-based phylogenetic analyses. As the Miocene form is only represented by one specimen in our sample, the shape, size and overlap of its morphospace relative to the other species remains speculative. Independently from the phylogeny, however, the fossil record reveals that representatives of the *M. niger* and *C. latirostris* lineage were already present in the Late Miocene of South America (e.g., Bona *et al.*, 2014, Scheyer and Delfino, 2016; this study), which is further supported by molecular-based time calibrations (Oaks, 2011). Together with *Globidentosuchus brachyrostris*, *Caiman australis* Bravard, 1858; Bona and Barrios, 2015, *Caiman brevirostris* Souza-Filho, 1987, *Caiman gasparinae* Bona and Carabajal, 2013, *Caiman lutescens* Roverto, 1912, *Caiman wannlangstoni* Salas-Gismondi *et al.*, 2015, *Gnatusuchus pebasensis* Salas-Gismondi *et al.*, 2015, *Kuttanacaiman iquitosensis* Salas-Gismondi *et al.*, 2015, *Mourasuchus arendsi* Bocquentin-Villanueva, 1984, *Purussaurus mirandai* Aguilera *et al*., 2006, *Paleosuchus* sp. Gray, 1862, *Purussaurus brasiliensis* Barbosa-Rodrigues, 1892 (see Scheyer *et al.*, 2013; Salas-Gismondi *et al.*, 2015; Scheyer and Delfino, 2016), *Melanosuchus* is a component of the high caimanine diversity that evolved in Amazonia since the Late Miocene.

6. Acknowledgements

TMS thanks Rodolfo Salas-Gismondi for the fruitful discussions and J. Carrillo (AMU) and R. Sánchez (STRI) for their support in Venezuela. H. Moreno (MCNC) is also to be thanked for providing access to the holotype specimen of *M. fisheri* and the Alcaldía Bolivariana del Municipio Urumaco is thanked for providing access to comparative caimanine material from the Urumaco Formation. We further thank Julia Desojo and Marcela Tomeo for helping with pictures and graphs, and four anonymous reviewers for helpful comments on the previous version of the manuscript. This work was supported by the Swiss National Science Foundation (grant no. 205321-162775 to TMS), the Deutsche Forschungsgemeinschaft (RA 1012/12-1 to CF), the Deutscher Akademischer Austauschdienst (grant no. 91546784 to CF) and the Agencia Nacional de Promoción Científica y Tecnológica (ANPCyT PICT-2012-0748).

7. Literature cited

Adams DC, Otárola-Castillo E. 2013. *geomorph*: an R package for the collection and analysis of geometric morphometric shape data. Methods Ecol Evol 4:393–399.

Aguilera OA, Riff D, Bocquentin-Villanueva JC. 2006. A new giant *Purusaurus* (Crocodyliformes, Alligatoridae) from the Upper Miocene Urumaco Formation, Venezuela. J Syst Palaeontol 4:221–232.

Anderson MJ. 2001. A new method for non-parametric multivariate analysis of variance. Austral Ecol 26:32–46.

Barbosa Rodrigues R. 1892. Les Reptiles fossiles de la vallée de l'Amazone. Vellosia-Contribuicões do Mus Bot do Amaz 2:41–46.

Benson RBJ, Domokos G, Várkonyi PL, Reisz RR. 2011. Shell geometry and habitat determination in extinct and extant turtles (Reptilia: Testudinata). Paleobiology 37:547–562.

Bocquentin-Villanueva JC. 1984. Un nuevo Nettosuchidae (Crocodylia, Eusuchia) proveniente da la Formación Urumaco (Mioceno Superior), Venezuela. Ameghiniana 21:3–8.

Bona P, Barrios F. 2015. The alligatoroidea of Argentina: an update of its fossil record. Publicación Electrónica la Asoc Paleontológica Argentina 15:143–158.

Bona P, Carabajal A. 2013. *Caiman gasparinae* sp. nov., a huge alligatorid (Caimaninae) from the late Miocene of Paraná, Argentina. Alcheringa 37:462–473.

Bona P, Desojo JB. 2011. Osteology and cranial musculature of *Caiman latirostris* (Crocodylia: Alligatoridae). J Morphol 272:780–795.

Bona P, Fernandez Blanco MV, Scheyer TM, Foth C. In press. Shedding light on the taxonomic diversity of the South American Miocene caimans: the status of *Melanosuchus fisheri* Medina, 1976 (Crocodylia, Alligatoroidea). Ameghiniana. doi:10.5710/AMGH.08.06.2017.3103

Bona P, Starck D, Galli C, Gasparini Z, Reguero M. 2014. *Caiman* cf. *latirostris* (Alligatoridae, Caimaninae) in the late Miocene Palo Pintado Formation, Salta Province, Argentina: paleogeographic and paleoenvironmental considerations. Ameghiniana 51:26–36.

Bookstein FL. 1991. Morphometric tools for landmark data. Cambridge: Cambridge University Press. 456 p.

Bravard A. 1858. Monografía de los terrenos marinos terciarios del Paraná. Paraná: Imprenta del Registro Oficial, Paraná. 107 p.

Brazaitis P. 1973. The identification of living crocodiles. Zoologica 58:59–105.

Brochu CA. 1999. Phylogenetics, taxonomy, and historical biogeography of Alligatoroidea. J Vertebr Paleontol 19:9–100.

Brochu CA. 2003. Phylogenetic approaches toward crocodylian history. Annu Rev Earth Planet Sci 31:357–397.

Brochu CA. 2004. Alligatorine phylogeny and the status of *Allognathosuchus* Mook, 1921. J Vertebr Paleontol 24:857–873.

Brochu CA. 2010. A new alligatorid from the lower Eocene Green River Formation of Wyoming and the origin of caimans. J Vertebr Paleontol 30:1109–1126.

Brochu CA. 2011. Phylogenetic relationships of *Necrosuchus ionensis* Simpson, 1937 and the early history of caimanines. Zool J Linn Soc 163:S228–S256.

Daudin FM. 1802. Histoire Naturelle, Générale et Particulière des Reptiles; ouvrage faisant suit à l'Histoire naturell générale et particulière, composée par Leclerc de Buffon; et rédigee par C.S. Sonnini, membre de plusieurs sociétés savantes. Vol. 2. Paris: F. Dufart. 432 p.

Drake AG. 2011. Dispelling dog dogma: an investigation of heterochrony in dogs using 3D geometric morphometric analysis of skull shape. Evol Dev 13:204–213.

Dryden IL, Mardia K V. 1998. Statistical shape analysis. New York: John Wiley. 347 p.

Fernandez Blanco M V, Cassini GH, Bona P. 2014. Variación morfológica craneana en *Caiman* (Alligatoridae, Caimaninae): estudio morfogeométrico de la ontogenia de las especies *Caiman latirostris* y *Caiman yacare*. Cs Morfol 16:16–30.

Foth C, Bona P, Desojo JB. 2015. Intraspecific variation in the skull morphology of the black caiman *Melanosuchus niger* (Alligatoridae, Caimaninae). Acta Zool 96:1–13.

Foth C, Ezcurra MD, Sookias RB, Brusatte SL, Butler RJ. 2016. Unappreciated diversification of stem archosaurs during the Middle Triassic predated the dominance of dinosaurs. BMC Evol Biol 16:188.

Foth C, Rabi M, Joyce WG. 2017. Skull shape variation in recent and fossil Testudinata and its relation to habitat and feeding ecology. Acta Zool 98: 310–325.

Gray JE. 1862. A synopsis of the species of alligators. Ann Mag Nat Hist 10:327–331.

Gunz P, Mitteroecker P, Neubauer S, Weber GW, Bookstein FL. 2009. Principles for the virtual reconstruction of hominin crania. J Hum Evol 57:48–62.

Hammer O, Harper DAT. 2006. Paleontological data analysis. Malden: Blackwell Publishing. 351 p.

Hammer O, Harper DAT, Ryan PD. 2001. PAST: paleontological statistics software package for education and data analysis. Palaeontol Electron 4:1–9.

Hastings AK, Reisser M, Scheyer TM. 2016. Character evolution and the origin of Caimaninae (Crocodylia) in the New World Tropics: new evidence from the Miocene of Panama and Venezuela. J Paleontol 90:317–332.

Hastings AK, Hellmund M. 2017. Evidence for prey preference partitioning in the middle Eocene high-diversity crocodylian assemblage of the Geiseltal-Fossillagerstätte, Germany utilizing skull shape analysis. Geol Mag 154:119–146.

Hrbek T, Vasconcelos WR, Rebelo G, Farias IP. 2008. Phylogenetic relationships of South American alligatorids and the *Caiman* of Madeira River. J Exp Zool 309A:588–599.

Jackson DA. 1993. Stopping rules in principal components analysis: a comparison of heuristical and statistical approaches. Ecology 74:2204–2214.

Kälin JA. 1933. Beiträge zur vergleichenden Osteologie des Crocodilidenschädels. Zool Jahrb 57:535–714.

Klingenberg CP. 2009. Morphometric integration and modularity in configurations of landmarks: tools for evaluating a priori hypotheses. Evol Dev 11:405–421.

Klingenberg CP. 2011. MorphoJ: an integrated software package for geometric morphometrics. Mol Ecol Resour 11:353–357.

Korkmaz S, Goksuluk D, Zararsiz G. 2014. MVN: an R package for assessing multivariate normality. R J 6:151–162.

Linnaeus C. 1758. Systema naturæ per regna tria naturæ, secundum classes, ordines, genera, species, cum characteribus, differentiis, synonymis, locis. Stockholm: Laurentius Salvius. 824 p.

Medina CJ. 1976. Crocodilian from the Late Tertiary of Northwestern Venezuela: *Melanosuchus fisheri* sp. nov. Breviora 438:1–14.

Monteiro LR, Cavalcanti MJ, Sommer HSJ. 1997. Comparative ontogenetic shape changes in the skull of *Caiman* species (Crocodylia, Alligatoridae). J Morphol 321:53–62.

Mook CC. 1921. Skull characters of recent Crocodilia, with notes on the affinities of the recent genera. Bull Am Museum Nat Hist 44:123–268.

Oaks JR. 2011. A time-calibrated species tree of Crocodylia reveals a recent radiation of the true crocodiles. Evolution (N Y) 65:3285–3297.

Okamoto KW, Langerhans RB, Rashid R, Amarasekare P. 2015. Microevolutionary patterns in the common caiman predict macroevolutionary trends across extant crocodilians. Biol J Linn Soc 116:834–846.

Pearcy A, Wijtten Z. 2010. Suggestions on photographing crocodile skulls for scientific purposes. Herpetol Rev 41:445–447.

Pierce SE, Angielczyk KD, Rayfield EJ. 2008. Patterns of morphospace occupation and mechanical performance in extant crocodilian skulls: a combined geometric morphometric and finite element modelling approach. J Morphol 269:840–864.

Piras P, Colangelo P, Adams DC, Buscalioni AD, Cubo J, Kotsakis T, Meloro C, Raia P. 2010. The *Gavialis-Tomistoma* debate: the contribution of skull ontogenetic allometry and growth trajectories to the study of crocodylian relationships. Evol Dev 12:568–579.

Poe S. 1996. Data set incongruence and the phylogeny of crocodilians. Syst Biol 45:393–414.

R Development Core Team. 2011. R: a language and environment for statistical computing. http://www.r-project.org.

Rohlf FJ. 2003. *tpsSmall*, is shape variation small?, version 1.19. Department of Ecology and Evolution, State University of New York at Stony Brook.

Rohlf FJ. 2004. *tpsUtil*, file utility program, version 1.26. Department of Ecology and Evolution, State University of New York at Stony Brook.

Rohlf FJ. 2005. *tpsDig*, digitize landmarks and outlines, version 2.05. Department of Ecology and Evolution, State University of New York at Stony Brook.

Rohlf FJ, Slice DE. 1990. Extensions of the Procrustes method for the optimal superimposition of landmarks. Syst Zool 39:40–59.

Rovereto C. 1912. Los cocodrilos fósiles en las capas del Paraná. An del Mus Nac Hist Nat Buenos Aires 22:339–368.

Salas-Gismondi R, Flynn J, Baby P, Tejada-Lara J V, Wesselingh FP, Antoine P-O. 2015. A Miocene hyperdiverse crocodylian community reveals peculiar trophic dynamics in proto-Amazonian mega-wetlands. Proc R Soc B 282:20142490.

Sánchez-Villagra MR, Aguilera OA. 2006. Neogene vertebrates from Urumaco, Falcón State, Venezuela: Diversity and significance. J Syst Palaeontol 4:213–220.

Scheyer TM, Aguilera OA, Delfino M, Fortier DC, Carlini AA, Sánchez R, Carrillo-Briceño JD, Quiroz L, Sánchez-Villagra MR. 2013. Crocodylian diversity peak and extinction in the late Cenozoic of the northern Neotropics. Nat Commun 4:1907.

Scheyer TM, Delfino M. 2016. The late Miocene caimanine fauna (Crocodylia: Alligatoroidea) of the Urumaco Formation, Venezuela. Palaeontol Electron 19.3.48A:1–57.

Souza-Filho JP. 1987. *Caiman brevirostris* sp. nov., um novo Alligatoridae da Formação Solimões (Pleistoceno) do Estado do Acre, Brasil. An X Congr Bras Paleontol Rio Janeiro 173–180.

Spix JB. 1825. Animalia nova sive Species novae lacertarum quas in itinere per Brasiliam annis MDCCCXVII–MDCCCXX jussu et auspiciis Maximiliani Josephi I. Leipzig: Bavariae Regis suscepto collegit et descripsit Dr. J.B. de Spix. T.O. Weigel. 26 p.

Stubbs TL, Pierce SE, Rayfield EJ, Anderson PSL. 2013. Morphological and biomechanical disparity of crocodile-line archosaurs following the end-Triassic extinction. Proc R Soc B 280:20131940.

Thorbjarnarson JB. 2010. Black Caiman *Melanosuchus niger*. In: Manolis SC, Stevenson C, editors. Crocodiles. Status survey and conservation action pan Darwin: Crocodile Specialist Group. p. 29–39.

Watanabe A, Slice DE. 2014. The utility of cranial ontogeny for phylogenetic inference: a case study in crocodylians using geometric morphometrics. J Evol Biol 27:1078–1092.

Wilberg EW. 2017. Investigating patterns of crocodyliform cranial disparity through the Mesozoic and Cenozoic. Zool J Linn Soc. published online:1-20.

Wilkinson PM, Rhodes WE. 1997. Growth rates of American alligators in coastal South Carolina. J Wildl Manage 61:397–402.

Young MT, Brusatte SL, Ruta M, Andrade MB. 2010. The evolution of Metriorhynchoidea (Mesoeucrocodylia, Thalattosuchia): an integrated approach using geometric morphometrics, analysis of disparity, and biomechanics. Zool J Linn Soc 158:801–859.

Zelditch ML, Swiderski DL, Sheets HD. 2012. Geometric morphometrics for biologists: a primer. Amsterdam: Elsevier Academic Press. 488p.

FIGURE and TABLE legends

TABLE 1. Differences of ontogenetic trajectories (one-way ANCOVA) of *Caiman yacare*, *C. crocodilus*, *C. latirostris* and *Melanosuchus niger* in dorsal and lateral views. *F*-values are shown in bold. Significant differences are shown with underlined *p*-values.

Dorsal view					
un-pooled	**Slope**	***C. crocodilus***	***C. yacare***	***C. latirostris***	***M. niger***
C. crocodilus	4.586		0.119	0.106	0.502
C. yacare	5.771	**2.471**		0.134	0.155
C. latirostris	6.848	**2.697**	**2.275**		0.04
M. niger	5.184	**0.455**	**2.045**	**4.308**	
pooled	**Slope**	***C. crocodilus***	***C. yacare***	***C. latirostris***	***M. niger***
C. crocodilus	3.648		0.062	0.048	0.24
C. yacare	4.674	**3.547**		0.065	0.505
C. latirostris	5.712	**4.067**	**3.483**		0.059
M. niger	4.449	**1.406**	**0.448**	**3.683**	
Lateral view					
un-pooled	**Slope**	***C. crocodilus***	***C. yacare***	***C. latirostris***	***M. niger***
C. crocodilus	3.158		0.011	0.011	0.002
C. yacare	4.799	**6.653**		0.011	0.293
C. latirostris	4.99	**6.613**	**6.813**		0.574
M. niger	5.216	**10.63**	**1.118**	**0.32**	
pooled	**Slope**	***C. crocodilus***	***C. yacare***	***C. latirostris***	***M. niger***
C. crocodilus	3.71		0.351	0.188	0.047
C. yacare	4.163	**0.878**		0.303	0.063
C. latirostris	4.544	**1.772**	**1.07**		0.584
M. niger	4.76	**4.086**	**3.515**	**0.302**	

TABLE 2. Probabilistic predictions for MCNC 243 showing the similarity to all extant jacarean caimanines (left) and *Caiman latirostris* and *Melanosuchus niger* (right) in dorsal and lateral views based on the Euclidean distances towards the centroids of the species morphospaces (defined by those principal components containing significant shape variation). Bold values indicate the highest similarity.

Dorsal view	**Procrustes coordinates**						
PC1–PC4	***C. crocodilus***	***C. yacare***	***C. latirostris***	***M. niger***	**PC1–PC3**	***C. latirostris***	***M. niger***
Average	0.167	0.213	0.237	**0.383**	Average	0.349	**0.651**
Median	0.169	0.221	0.262	**0.348**	Median	0.407	**0.593**
	Un-pooled, non-allometric residuals						
PC1–PC4	***C. crocodilus***	***C. yacare***	***C. latirostris***	***M. niger***	**PC1 and PC4**	***C. latirostris***	***M. niger***
Average	0.157	0.209	0.287	**0.346**	Average	**0.718**	0.282
Median	0.154	0.205	**0.339**	0.302	Median	**0.588**	0.412
	Pooled, non-allometric residuals						
PC1–PC3	***C. crocodilus***	***C. yacare***	***C. latirostris***	***M. niger***	**PC1 and PC4**	***C. latirostris***	***M. niger***
Average	0.188	0.207	0.279	**0.326**	Average	0.44	**0.561**
Median	0.182	0.208	0.299	**0.312**	Median	0.443	**0.557**
Lateral view	**Procrustes coordinates**						
PC1–PC3	***C. crocodilus***	***C. yacare***	***C. latirostris***	***M. niger***	**PC1**	***C. latirostris***	***M. niger***
Average	0.161	0.236	0.282	**0.321**	Average	0.31	**0.69**
Median	0.165	0.238	**0.307**	0.29	Median	0.332	**0.668**
	Un-pooled, non-allometric residuals						
PC1–PC3	***C. crocodilus***	***C. yacare***	***C. latirostris***	***M. niger***	**PC1**	***C. latirostris***	***M. niger***
Average	0.158	0.227	0.275	**0.34**	Average	0.437	**0.563**
Median	0.156	0.227	0.301	**0.317**	Median	0.466	**0.534**
	Pooled, non-allometric residuals						
PC1–PC3	***C. crocodilus***	***C. yacare***	***C. latirostris***	***M. niger***	**PC1**	***C. latirostris***	***M. niger***
Average	0.178	0.252	**0.324**	0.247	Average	**0.561**	0.439
Median	0.176	0.243	**0.345**	0.236	Median	**0.58**	0.42

TABLE 3. Results of the Discriminant Function Analysis (DFA) and Canonical Variance Analysis (CVA) in dorsal view, showing the difference of MCNC 243 to all extant jacarean caimanines (left) and *Caiman latirostris* and *Melanosuchus niger* (right). Bold *p*-values show non-significant values, indicating no statistical differences.

Procrustes coordinates						
DFA	***C. crocodilus***	***C. yacare***	***C. latirostris***	***M. niger***	***C. latirostris***	***M. niger***
Procrustes distance	0.101	0.087	0.083	0.069	0.083	0.069
p-value	0.022	0.003	0.035	**0.151**	0.042	**0.153**
Mahalanobis distance	18.659	83.83	19.343	145.231	19.375	144.826
p-value	0.015	0.009	0.019	0.015	0.014	0.003
CVA	***C. crocodilus***	***C. yacare***	***C. latirostris***	***M. niger***	***C. latirostris***	***M. niger***
Procrustes distance	0.101	0.087	0.083	0.069	0.083	0.069
p-value	0.003	0	0.032	**0.144**	0.049	**0.14**
Mahalanobis distance	28.024	26.969	25.672	25.448	36.875	36.903
p-value	0.003	0.01	0.024	0.02	0.017	0.006
Un-pooled, non-allometric residuals						
DFA	***C. crocodilus***	***C. yacare***	***C. latirostris***	***M. niger***	***C. latirostris***	***M. niger***
Procrustes distance	0.101	0.087	0.078	0.071	0.077	0.069
p-value	0.006	0.006	**0.058**	**0.108**	**0.078**	**0.112**
Mahalanobis distance	16.184	75.242	14.764	92.761	17.851	88.049
p-value	0.035	0.001	**0.053**	0.002	0.003	0.014
CVA	***C. crocodilus***	***C. yacare***	***C. latirostris***	***M. niger***	***C. latirostris***	***M. niger***
Procrustes distance	0.101	0.087	0.078	0.071	0.077	0.069
p-value	0.015	0.013	0.05	**0.102**	**0.074**	**0.092**
Mahalanobis distance	27.258	26.128	24.713	25.154	36.218	36.001
p-value	0.014	0.004	0.019	0.008	0.028	0.02
Pooled, non-allometric residuals						
DFA	***C. crocodilus***	***C. yacare***	***C. latirostris***	***M. niger***	***C. latirostris***	***M. niger***
Procrustes distance	0.102	0.095	0.084	0.076	0.086	0.075
p-value	0.006	0.003	0.045	0.04	0.014	0.032
Mahalanobis distance	17.084	73.415	23.539	71.265	20.173	58.771
p-value	0.001	0.004	0.021	0.015	0.002	0.002
CVA	***C. crocodilus***	***C. yacare***	***C. latirostris***	***M. niger***	***C. latirostris***	***M. niger***
Procrustes distance	0.102	0.095	0.084	0.076	0.086	0.075
p-value	0.026	0.001	0.041	0.03	0.007	0.022
Mahalanobis distance	28.335	27.431	26.139	25.717	39.412	36.958
p-value	0.008	0.002	0.023	0.017	0.003	0.007

TABLE 4. Results of the Discriminant Function Analysis (DFA) and Canonical Variance Analysis (CVA) in lateral view, showing the difference of MCNC 243 to all extant jacarean caimanines (left) and *Caiman latirostris* and *Melanosuchus niger* (right).

Procrustes coordinates						
DFA	***C. crocodilus***	***C. yacare***	***C. latirostris***	***M. niger***	***C. latirostris***	***M. niger***
Procrustes distance	0.119	0.097	0.091	0.086	0.091	0.086
p-value	0.006	0.005	**0.189**	**0.141**	**0.182**	**0.123**
Mahalanobis distance	214.047	37.702	52.386	50.825	53.263	50.393
p-value	0.017	0.005	**0.068**	0.042	**0.067**	0.029
CVA	***C. crocodilus***	***C. yacare***	***C. latirostris***	***M. niger***	***C. latirostris***	***M. niger***
Procrustes distance	0.119	0.097	0.091	0.086	0.091	0.086
p-value	0.01	0.007	**0.189**	**0.129**	**0.185**	**0.112**
Mahalanobis distance	20.312	19.825	21.293	19.23	22.861	22.129
p-value	0.026	0.005	0.002	0.022	0.028	0.016
Un-pooled, non-allometric residuals						
DFA	***C. crocodilus***	***C. yacare***	***C. latirostris***	***M. niger***	***C. latirostris***	***M. niger***
Procrustes distance	0.116	0.099	0.091	0.086	0.092	0.078
p-value	0.008	0	**0.055**	0.009	**0.128**	**0.103**
Mahalanobis distance	137.517	35.782	47.987	42.782	47.033	39.356
p-value	0.032	0.001	**0.111**	**0.061**	**0.105**	**0.064**
CVA	***C. crocodilus***	***C. yacare***	***C. latirostris***	***M. niger***	***C. latirostris***	***M. niger***
Procrustes distance	0.117	0.099	0.091	0.086	0.092	0.078
p-value	0.018	0.015	0.066	0.011	**0.104**	**0.086**
Mahalanobis distance	20.724	20.335	21.031	19.669	22.928	22.211
p-value	0.011	0.009	0.006	0.005	0.013	0.002
Pooled, non-allometric residuals						
DFA	***C. crocodilus***	***C. yacare***	***C. latirostris***	***M. niger***	***C. latirostris***	***M. niger***
Procrustes distance	0.116	0.099	0.09	0.099	0.09	0.096
p-value	0.004	0.005	**0.06**	0.001	**0.09**	0.005
Mahalanobis distance	163.084	33.383	48.044	49.573	66.518	51.184
p-value	0.023	0.013	0.037	**0.068**	0.042	0.037
CVA	***C. crocodilus***	***C. yacare***	***C. latirostris***	***M. niger***	***C. latirostris***	***M. niger***
Procrustes distance	0.116	0.099	0.09	0.099	0.09	0.096
p-value	0	0.008	**0.081**	0.004	**0.089**	0.01
Mahalanobis distance	20.751	20.365	21.32	20.906	23.211	24.686
p-value	0	0.011	0.002	0.001	0.016	0.012

FIGURE 1. Skull morphology of jacarean caimanines. Cranium in dorsal view showing the different orbital shape in **A.** *Caiman latirostris* (MACN 7375), **B.** MCNC 243, and **C.** *Melanosuchus niger* (ZSM 86/1911). Shape of the dorsal jugal margin in **D.** *Caiman latirostris* (MACN 7375), **E.** MCNC 243, and **F.** *Melanosuchus niger* (ZSM 68/1911). Scale bar 5 cm.

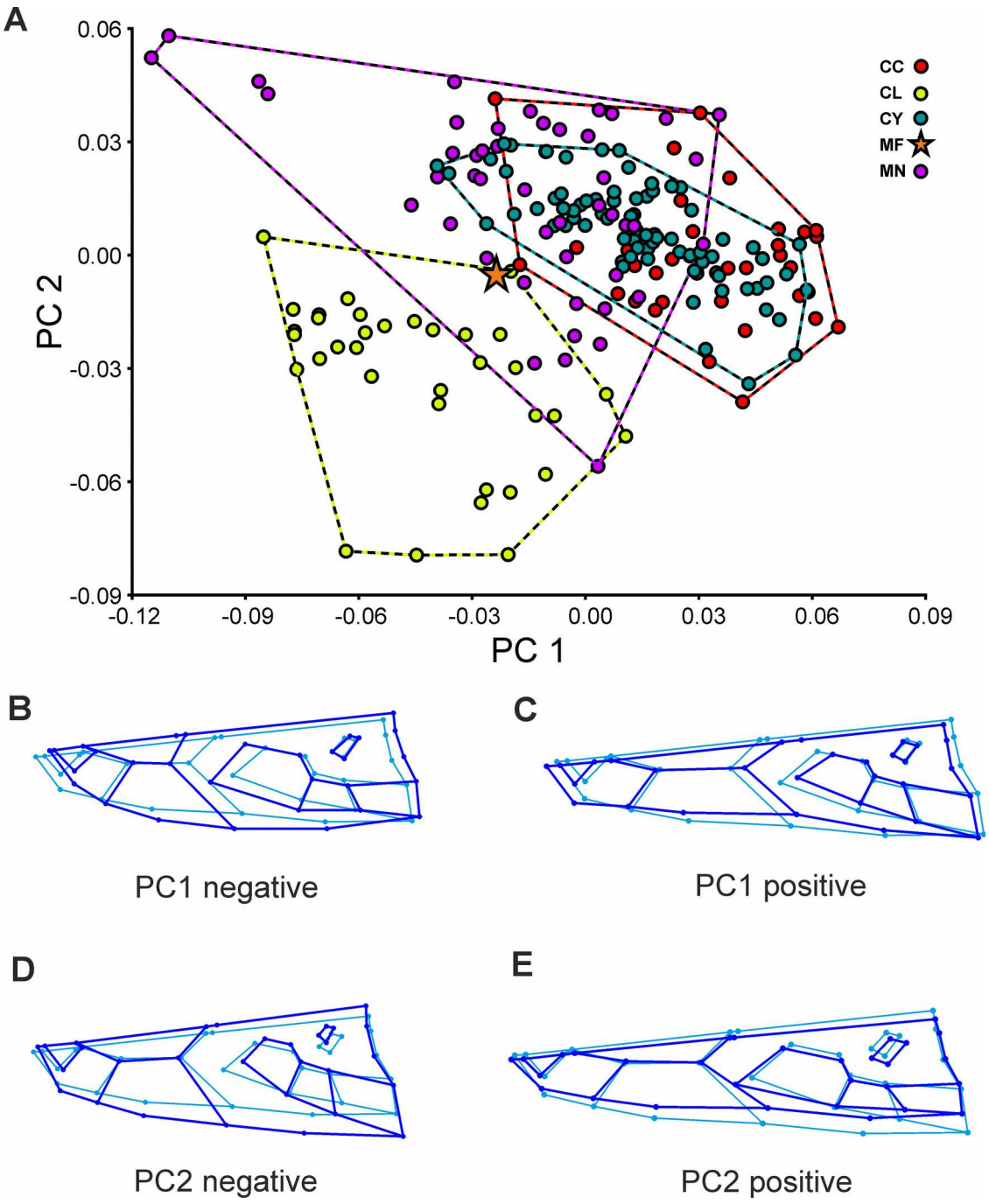

FIGURE 2. Results of **A.** the principal component analysis and **B–E.** major shape variation in dorsal view. Red circle (*Caiman crocodilus*, CC), violet circle (*Melanosuchus niger*, MN), orange star (MCNC 243, MF), dark green circle (*C. yacare*, CY), yellow circle (*C. latirostris*, CL). Blue wireframes show major shape variation of the first two principal components compared to the consensus shape shown in cyan.

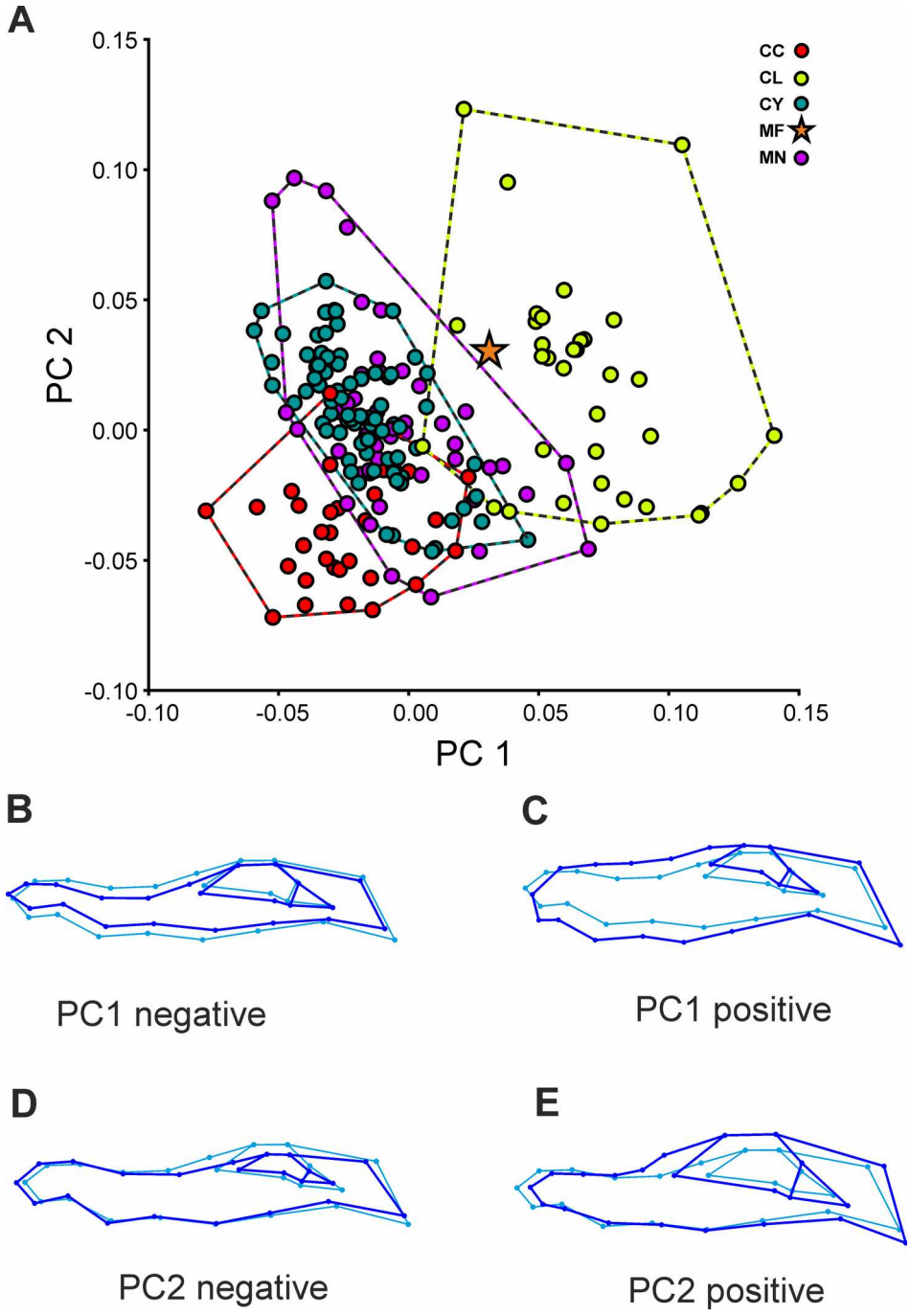

FIGURE 3. Results of **A.** the principal component analysis and **B–E.** major shape variation in lateral view. Red circle (*Caiman crocodilus*, CC), violet circle (*Melanosuchus niger*, MN), orange star (MCNC 243, MF), dark green circle (*C. yacare*, CY), yellow circle (*C. latirostris*, CL). Blue wireframes show major shape variation of the first two principal components compared to the consensus shape shown in cyan.

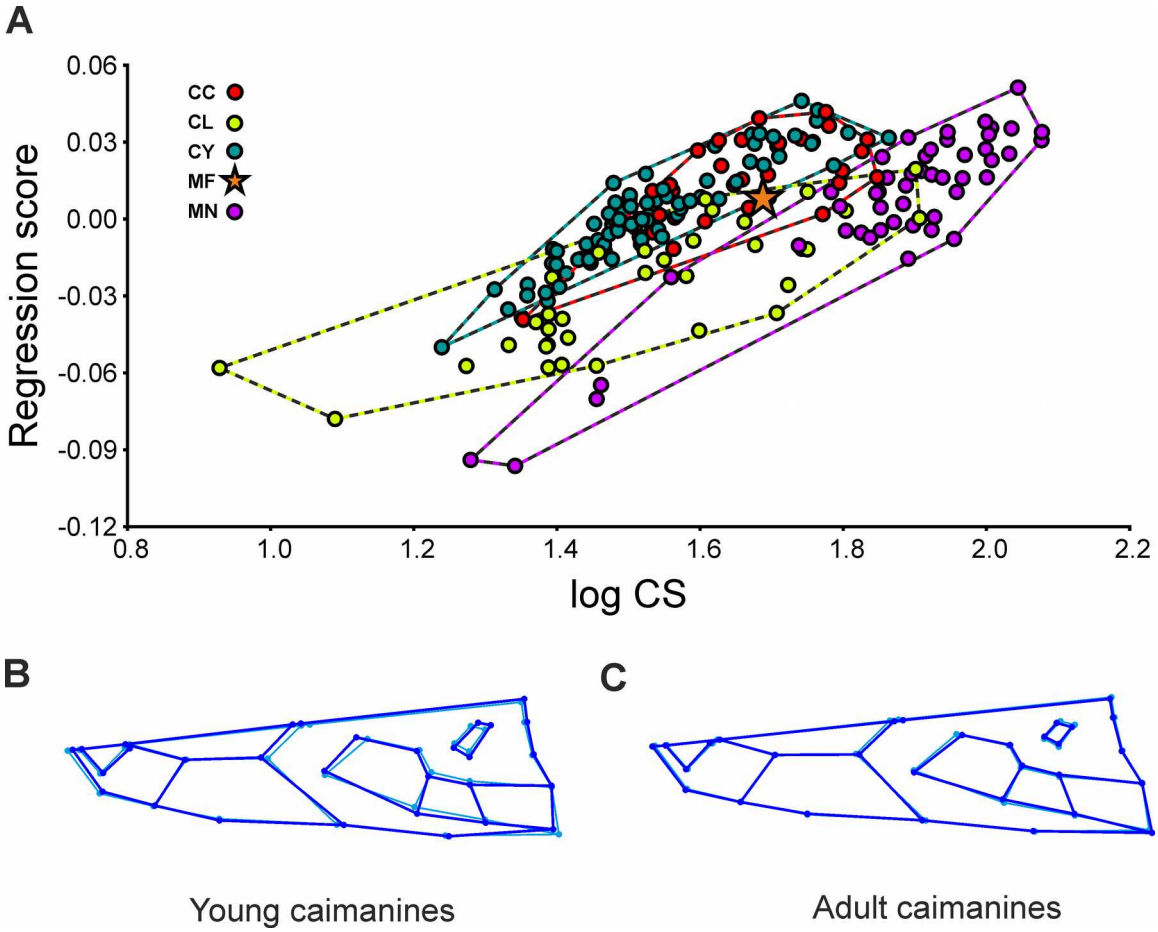

FIGURE 4. Results of **A.** the Regression Analysis and **B–C.** major shape variation during ontogeny in dorsal view. Red circle (*Caiman crocodilus*, CC), violet circle (*Melanosuchus niger*, MN), orange star (MCNC 243, MF), dark green circle (*C. yacare*, CY), yellow circle (*C. latirostris*, CL). Blue wireframes show major shape variation during ontogeny compared to the consensus shape shown in cyan.

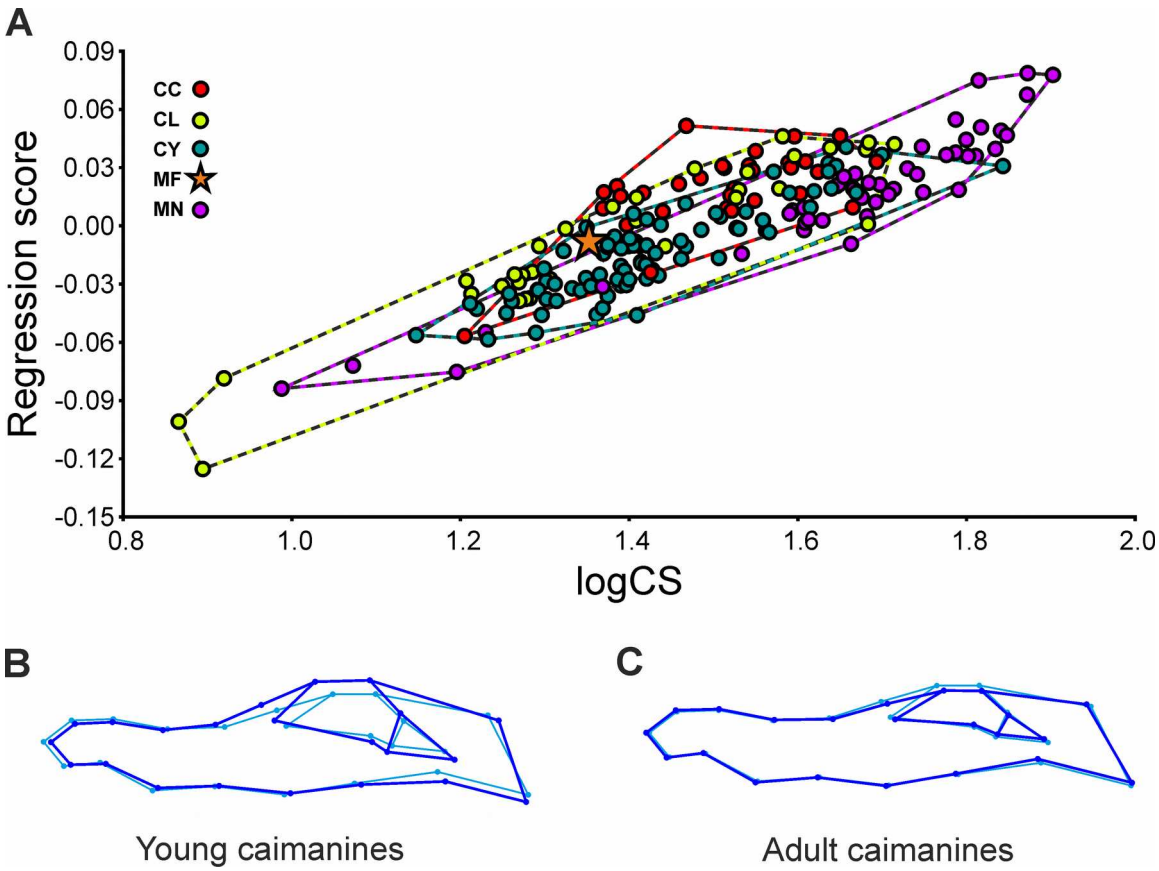

FIGURE 5. Results of **A.** the Regression Analysis and **B–C.** major shape variation during ontogeny in lateral view. Red circle (*Caiman crocodilus*, CC), violet circle (*Melanosuchus niger*, MN), orange star (MCNC 243, MF), dark green circle (*C. yacare*, CY), yellow circle (*C. latirostris*, CL). Blue wireframes show major shape variation during ontogeny compared to the consensus shape shown in cyan.